ELSEVIER

Measurement of the mass and width of the W boson in e⁺e⁻ collisions at $\sqrt{s} = 189$ GeV

DELPHI Collaboration

P. Abreu [u], W. Adam [aw], T. Adye [aj], P. Adzic [k], Z. Albrecht [r], T. Alderweireld [b],
G.D. Alekseev [q], R. Alemany [i], T. Allmendinger [r], P.P. Allport [v], S. Almehed [x],
U. Amaldi [ab], N. Amapane [ar], S. Amato [at], E. Anashkin [ai], E.G. Anassontzis [c],
P. Andersson [aq], A. Andreazza [aa], S. Andringa [u], N. Anjos [u], P. Antilogus [y], W.-D. Apel [r],
Y. Arnoud [o], B. Åsman [aq], J.-E. Augustin [w], A. Augustinus [i], P. Baillon [i],
A. Ballestrero [ar], P. Bambade [i,t], F. Barao [u], G. Barbiellini [as], R. Barbier [y], D.Y. Bardin [q],
G. Barker [r], A. Baroncelli [al], M. Battaglia [p], M. Baubillier [w], K.-H. Becks [ay], M. Begalli [f],
A. Behrmann [ay], T.F. Bellunato [i], Yu. Belokopytov [i], K. Belous [ao], N.C. Benekos [ae],
A.C. Benvenuti [e], C. Berat [o], M. Berggren [w], L. Berntzon [aq], D. Bertrand [b],
M. Besancon [am], N. Besson [am], M.S. Bilenky [q], D. Bloch [j], H.M. Blom [ad], L. Bol [r],
M. Bonesini [ab], M. Boonekamp [am], P.S.L. Booth [v], G. Borisov [t], C. Bosio [al], O. Botner [au],
E. Boudinov [ad], B. Bouquet [t], T.J.V. Bowcock [v], I. Boyko [q], I. Bozovic [k], M. Bracko [ap],
P. Branchini [al], R.A. Brenner [au], P. Bruckman [i], J.-M. Brunet [h], L. Bugge [af],
P. Buschmann [ay], M. Caccia [aa], M. Calvi [ab], T. Camporesi [i], V. Canale [ak], F. Carena [i],
L. Carroll [v], C. Caso [n], M.V. Castillo Gimenez [av], A. Cattai [i], F.R. Cavallo [e],
M. Chapkin [ao], Ph. Charpentier [i], P. Checchia [ai], G.A. Chelkov [q], R. Chierici [ar],
P. Chliapnikov [ao], P. Chochula [g], V. Chorowicz [y], J. Chudoba [ac], K. Cieslik [s], P. Collins [i],
R. Contri [n], E. Cortina [av], G. Cosme [t], F. Cossutti [i], M. Costa [av], H.B. Crawley [a],
D. Crennell [aj], J. Croix [j], G. Crosetti [n], J. Cuevas Maestro [ag], S. Czellar [p], J. D'Hondt [b],
J. Dalmau [aq], M. Davenport [i], W. Da Silva [w], G. Della Ricca [as], P. Delpierre [z],
N. Demaria [ar], A. De Angelis [as], W. De Boer [r], C. De Clercq [b], B. De Lotto [as],
A. De Min [i], L. De Paula [at], H. Dijkstra [i], L. Di Ciaccio [ak], K. Doroba [ax], M. Dracos [j],
J. Drees [ay], M. Dris [ae], G. Eigen [d], T. Ekelof [au], M. Ellert [au], M. Elsing [i], J.-P. Engel [j],
M. Espirito Santo [i], G. Fanourakis [k], D. Fassouliotis [k], M. Feindt [r], J. Fernandez [an],
A. Ferrer [av], E. Ferrer-Ribas [t], F. Ferro [n], A. Firestone [a], U. Flagmeyer [ay], H. Foeth [i],
E. Fokitis [ae], F. Fontanelli [n], B. Franek [aj], A.G. Frodesen [d], R. Fruhwirth [aw],
F. Fulda-Quenzer [t], J. Fuster [av], A. Galloni [v], D. Gamba [ar], S. Gamblin [t],
M. Gandelman [at], C. Garcia [av], C. Gaspar [i], M. Gaspar [at], U. Gasparini [ai], Ph. Gavillet [i],
E.N. Gazis [ae], D. Gele [j], T. Geralis [k], N. Ghodbane [y], I. Gil [av], F. Glege [ay], R. Gokieli [i,ax],

B. Golob [i,ap], G. Gomez-Ceballos [an], P. Goncalves [u], I. Gonzalez Caballero [an],
G. Gopal [aj], L. Gorn [a], Yu. Gouz [ao], V. Gracco [n], J. Grahl [a], E. Graziani [al], G. Grosdidier [t],
K. Grzelak [ax], J. Guy [aj], C. Haag [r], F. Hahn [i], S. Hahn [ay], S. Haider [i], A. Hallgren [au],
K. Hamacher [ay], J. Hansen [af], F.J. Harris [ah], S. Haug [af], F. Hauler [r], V. Hedberg [i,x],
S. Heising [r], J.J. Hernandez [av], P. Herquet [b], H. Herr [i], O. Hertz [r], E. Higon [av],
S.-O. Holmgren [aq], P.J. Holt [ah], S. Hoorelbeke [b], M. Houlden [v], J. Hrubec [aw],
G.J. Hughes [v], K. Hultqvist [i,aq], J.N. Jackson [v], R. Jacobsson [i], P. Jalocha [s],
Ch. Jarlskog [x], G. Jarlskog [x], P. Jarry [am], B. Jean-Marie [t], D. Jeans [ah], E.K. Johansson [aq],
P. Jonsson [y], C. Joram [i], P. Juillot [j], L. Jungermann [r], F. Kapusta [w], K. Karafasoulis [k],
S. Katsanevas [y], E.C. Katsoufis [ae], R. Keranen [r], G. Kernel [ap], B.P. Kersevan [ap],
Yu. Khokhlov [ao], B.A. Khomenko [q], N.N. Khovanski [q], A. Kiiskinen [p], B. King [v],
A. Kinvig [v], N.J. Kjaer [i], O. Klapp [ay], P. Kluit [ad], P. Kokkinias [k], V. Kostioukhine [ao],
C. Kourkoumelis [c], O. Kouznetsov [q], M. Krammer [aw], E. Kriznic [ap], Z. Krumstein [q],
P. Kubinec [g], M. Kucharczyk [s], J. Kurowska [ax], J.W. Lamsa [a], J.-P. Laugier [am],
G. Leder [aw], F. Ledroit [o], L. Leinonen [aq], A. Leisos [k], R. Leitner [ac], G. Lenzen [ay],
V. Lepeltier [t], T. Lesiak [s], M. Lethuillier [y], J. Libby [ah], W. Liebig [ay], D. Liko [i],
A. Lipniacka [aq], I. Lippi [ai], J.G. Loken [ah], J.H. Lopes [at], J.M. Lopez [an],
R. Lopez-Fernandez [o], D. Loukas [k], P. Lutz [am], L. Lyons [ah], J. MacNaughton [aw],
J.R. Mahon [f], A. Maio [u], A. Malek [ay], S. Maltezos [ae], V. Malychev [q], F. Mandl [aw],
J. Marco [an], R. Marco [an], B. Marechal [at], M. Margoni [ai], J.-C. Marin [i], C. Mariotti [i],
A. Markou [k], C. Martinez-Rivero [i], S. Marti i Garcia [i], J. Masik [l],
N. Mastroyiannopoulos [k], F. Matorras [an], C. Matteuzzi [ab], G. Matthiae [ak],
F. Mazzucato [ai,m], M. Mazzucato [ai], M. Mc Cubbin [v], R. Mc Kay [a], R. Mc Nulty [v],
G. Mc Pherson [v], E. Merle [o], C. Meroni [aa], W.T. Meyer [a], E. Migliore [i], L. Mirabito [y],
W.A. Mitaroff [aw], U. Mjoernmark [x], T. Moa [aq], M. Moch [r], K. Moenig [i,1], M.R. Monge [n],
J. Montenegro [ad], D. Moraes [at], P. Morettini [n], G. Morton [ah], U. Mueller [ay], K. Muenich [ay],
M. Mulders [ad], L.M. Mundim [f], W.J. Murray [aj], B. Muryn [s], G. Myatt [ah], T. Myklebust [af],
M. Nassiakou [k], F.L. Navarria [e], K. Nawrocki [ax], P. Negri [ab], S. Nemecek [l], N. Neufeld [aw],
R. Nicolaidou [am], P. Niezurawski [ax], M. Nikolenko [j,q], V. Nomokonov [p], A. Nygren [x],
V. Obraztsov [ao], A.G. Olshevski [q], A. Onofre [u], R. Orava [p], K. Osterberg [i], A. Ouraou [am],
A. Oyanguren [av], M. Paganoni [ab], S. Paiano [e], R. Pain [w], R. Paiva [u], J. Palacios [ah],
H. Palka [s], Th.D. Papadopoulou [ae], L. Pape [i], C. Parkes [i], F. Parodi [n], U. Parzefall [v],
A. Passeri [al], O. Passon [ay], L. Peralta [u], V. Perepelitsa [av], M. Pernicka [aw], A. Perrotta [e],
C. Petridou [as], A. Petrolini [n], H.T. Phillips [aj], F. Pierre [am], M. Pimenta [u], E. Piotto [aa],
T. Podobnik [ap], V. Poireau [am], M.E. Pol [f], G. Polok [s], P. Poropat [as], V. Pozdniakov [q],
P. Privitera [ak], N. Pukhaeva [q], A. Pullia [ab], D. Radojicic [ah], S. Ragazzi [ab], H. Rahmani [ae],
A.L. Read [af], P. Rebecchi [i], N.G. Redaelli [ab], M. Regler [aw], J. Rehn [r], D. Reid [ad],
R. Reinhardt [ay], P.B. Renton [ah], L.K. Resvanis [c], F. Richard [t], J. Ridky [l], G. Rinaudo [ar],

I. Ripp-Baudot [j], A. Romero [ar], P. Ronchese [ai], E.I. Rosenberg [a], P. Rosinsky [g],
P. Roudeau [t], T. Rovelli [e], V. Ruhlmann-Kleider [am], A. Ruiz [an], H. Saarikko [p],
Y. Sacquin [am], A. Sadovsky [q], G. Sajot [o], L. Salmi [p], J. Salt [av], D. Sampsonidis [k],
M. Sannino [n], A. Savoy-Navarro [w], C. Schwanda [aw], Ph. Schwemling [w], B. Schwering [ay],
U. Schwickerath [r], F. Scuri [as], Y. Sedykh [q], A.M. Segar [ah], R. Sekulin [aj], G. Sette [n],
R.C. Shellard [f], M. Siebel [ay], L. Simard [am], F. Simonetto [ai], A.N. Sisakian [q], G. Smadja [y],
N. Smirnov [ao], O. Smirnova [x], G.R. Smith [aj], A. Sokolov [ao], O. Solovianov [ao],
A. Sopczak [r], R. Sosnowski [ax], T. Spassov [i], E. Spiriti [al], S. Squarcia [n], C. Stanescu [al],
M. Stanitzki [r], K. Stevenson [ah], A. Stocchi [t], J. Strauss [aw], R. Strub [j], B. Stugu [d],
M. Szczekowski [ax], M. Szeptycka [ax], T. Tabarelli [ab], A. Taffard [v], F. Tegenfeldt [au],
F. Terranova [ab], J. Timmermans [ad], N. Tinti [e], L.G. Tkatchev [q], M. Tobin [v], S. Todorova [i],
B. Tome [u], A. Tonazzo [i], L. Tortora [al], P. Tortosa [av], D. Treille [i], G. Tristram [h],
M. Trochimczuk [ax], C. Troncon [aa], M.-L. Turluer [am], I.A. Tyapkin [q], P. Tyapkin [x],
S. Tzamarias [k], O. Ullaland [i], V. Uvarov [ao], G. Valenti [i,e], E. Vallazza [as],
C. Vander Velde [b], P. Van Dam [ad], W. Van den Boeck [b], W.K. Van Doninck [b],
J. Van Eldik [i,ad], A. Van Lysebetten [b], N. van Remortel [b], I. Van Vulpen [ad], G. Vegni [aa],
L. Ventura [ai], W. Venus [aj,i], F. Verbeure [b], P. Verdier [y], M. Verlato [ai], L.S. Vertogradov [q],
V. Verzi [aa], D. Vilanova [am], L. Vitale [as], E. Vlasov [ao], A.S. Vodopyanov [q], G. Voulgaris [c],
V. Vrba [l], H. Wahlen [ay], A.J. Washbrook [v], C. Weiser [i], D. Wicke [i], J.H. Wickens [b],
G.R. Wilkinson [ah], M. Winter [j], M. Witek [s], G. Wolf [i], J. Yi [a], O. Yushchenko [ao],
A. Zalewska [s], P. Zalewski [ax], D. Zavrtanik [ap], E. Zevgolatakos [k], N.I. Zimin [q,x],
A. Zintchenko [q], Ph. Zoller [j], G. Zumerle [ai], M. Zupan [k]

[a] *Department of Physics and Astronomy, Iowa State University, Ames, IA 50011-3160, USA*
[b] *Physics Department, Univ. Instelling Antwerpen, Universiteitsplein 1, B-2610 Antwerpen*
and IIHE, ULB-VUB, Pleinlaan 2, B-1050 Brussels
and Faculté des Sciences, Univ. de l'Etat Mons, Av. Maistriau 19, B-7000 Mons, Belgium
[c] *Physics Laboratory, University of Athens, Solonos Str. 104, GR-10680 Athens, Greece*
[d] *Department of Physics, University of Bergen, Allégaten 55, NO-5007 Bergen, Norway*
[e] *Dipartimento di Fisica, Università di Bologna and INFN, Via Irnerio 46, IT-40126 Bologna, Italy*
[f] *Centro Brasileiro de Pesquisas Físicas, rua Xavier Sigaud 150, BR-22290 Rio de Janeiro*
and Depto. de Física, Pont. Univ. Católica, C.P. 38071 BR-22453 Rio de Janeiro
and Inst. de Física, Univ. Estadual do Rio de Janeiro, rua São Francisco Xavier 524, Rio de Janeiro, Brazil
[g] *Comenius University, Faculty of Mathematics and Physics, Mlynska Dolina, SK-84215 Bratislava, Slovakia*
[h] *Collège de France, Lab. de Physique Corpusculaire, IN2P3-CNRS, FR-75231 Paris Cedex 05, France*
[i] *CERN, CH-1211 Geneva 23, Switzerland*
[j] *Institut de Recherches Subatomiques, IN2P3 - CNRS/ULP - BP20, FR-67037 Strasbourg Cedex, France*
[k] *Institute of Nuclear Physics, N.C.S.R. Demokritos, P.O. Box 60228, GR-15310 Athens, Greece*
[l] *FZU, Inst. of Phys. of the C.A.S. High Energy Physics Division, Na Slovance 2, CZ-180 40, Praha 8, Czech Republic*
[m] *Currently at DPNC, University of Geneva, Quai Ernest-Ansermet 24, CH-1211, Geneva, Switzerland*
[n] *Dipartimento di Fisica, Università di Genova and INFN, Via Dodecaneso 33, IT-16146 Genova, Italy*
[o] *Institut des Sciences Nucléaires, IN2P3-CNRS, Université de Grenoble 1, FR-38026 Grenoble Cedex, France*
[p] *Helsinki Institute of Physics, HIP, P.O. Box 9, FI-00014 Helsinki, Finland*
[q] *Joint Institute for Nuclear Research, Dubna, Head Post Office, P.O. Box 79, RU-101 000 Moscow, Russian Federation*
[r] *Institut für Experimentelle Kernphysik, Universität Karlsruhe, Postfach 6980, DE-76128 Karlsruhe, Germany*
[s] *Institute of Nuclear Physics and University of Mining and Metallurgy, Ul. Kawiory 26a, PL-30055 Krakow, Poland*
[t] *Université de Paris-Sud, Lab. de l'Accélérateur Linéaire, IN2P3-CNRS, Bât. 200, FR-91405 Orsay Cedex, France*

[u] LIP, IST, FCUL - Av. Elias Garcia, 14-1°, PT-1000 Lisboa Codex, Portugal
[v] Department of Physics, University of Liverpool, P.O. Box 147, Liverpool L69 3BX, UK
[w] LPNHE, IN2P3-CNRS, Univ. Paris VI et VII, Tour 33 (RdC), 4 place Jussieu, FR-75252 Paris Cedex 05, France
[x] Department of Physics, University of Lund, Sölvegatan 14, SE-223 63 Lund, Sweden
[y] Université Claude Bernard de Lyon, IPNL, IN2P3-CNRS, FR-69622 Villeurbanne Cedex, France
[z] Univ. d'Aix - Marseille II - CPP, IN2P3-CNRS, FR-13288 Marseille Cedex 09, France
[aa] Dipartimento di Fisica, Università di Milano and INFN-MILANO, Via Celoria 16, IT-20133 Milan, Italy
[ab] Dipartimento di Fisica, Univ. di Milano-Bicocca and INFN-MILANO, Piazza delle Scienze 2, IT-20126 Milan, Italy
[ac] IPNP of MFF, Charles Univ., Areal MFF, V Holesovickach 2, CZ-180 00, Praha 8, Czech Republic
[ad] NIKHEF, Postbus 41882, NL-1009 DB Amsterdam, The Netherlands
[ae] National Technical University, Physics Department, Zografou Campus, GR-15773 Athens, Greece
[af] Physics Department, University of Oslo, Blindern, NO-1000 Oslo 3, Norway
[ag] Dpto. Fisica, Univ. Oviedo, Avda. Calvo Sotelo s/n, ES-33007 Oviedo, Spain
[ah] Department of Physics, University of Oxford, Keble Road, Oxford OX1 3RH, UK
[ai] Dipartimento di Fisica, Università di Padova and INFN, Via Marzolo 8, IT-35131 Padua, Italy
[aj] Rutherford Appleton Laboratory, Chilton, Didcot OX11 0QX, UK
[ak] Dipartimento di Fisica, Università di Roma II and INFN, Tor Vergata, IT-00173 Rome, Italy
[al] Dipartimento di Fisica, Università di Roma III and INFN, Via della Vasca Navale 84, IT-00146 Rome, Italy
[am] DAPNIA/Service de Physique des Particules, CEA-Saclay, FR-91191 Gif-sur-Yvette Cedex, France
[an] Instituto de Fisica de Cantabria (CSIC-UC), Avda. los Castros s/n, ES-39006 Santander, Spain
[ao] Inst. for High Energy Physics, Serpukov P.O. Box 35, Protvino (Moscow Region), Russian Federation
[ap] J. Stefan Institute, Jamova 39, SI-1000 Ljubljana
and Laboratory for Astroparticle Physics, Nova Gorica Polytechnic, Kostanjeviska 16a, SI-5000 Nova Gorica
and Department of Physics, University of Ljubljana, SI-1000 Ljubljana, Slovenia
[aq] Fysikum, Stockholm University, Box 6730, SE-113 85 Stockholm, Sweden
[ar] Dipartimento di Fisica Sperimentale, Università di Torino and INFN, Via P. Giuria 1, IT-10125 Turin, Italy
[as] Dipartimento di Fisica, Università di Trieste and INFN, Via A. Valerio 2, IT-34127 Trieste
and Istituto di Fisica, Università di Udine, IT-33100 Udine, Italy
[at] Univ. Federal do Rio de Janeiro, C.P. 68528 Cidade Univ., Ilha do Fundão BR-21945-970 Rio de Janeiro, Brazil
[au] Department of Radiation Sciences, University of Uppsala, P.O. Box 535, SE-751 21 Uppsala, Sweden
[av] IFIC, Valencia-CSIC, and D.F.A.M.N., U. de Valencia, Avda. Dr. Moliner 50, ES-46100 Burjassot (Valencia), Spain
[aw] Institut für Hochenergiephysik, Österr. Akad. d. Wissensch., Nikolsdorfergasse 18, AT-1050 Vienna, Austria
[ax] Inst. Nuclear Studies and University of Warsaw, Ul. Hoza 69, PL-00681 Warsaw, Poland
[ay] Fachbereich Physik, University of Wuppertal, Postfach 100 127, DE-42097 Wuppertal, Germany

Abstract

A measurement of the W mass and width has been performed by the DELPHI Collaboration using the data collected during 1998. The data sample has an integrated luminosity of 155 pb^{-1} and an average centre-of-mass energy of 188.6 GeV. Results are obtained by applying the method of direct reconstruction of the mass of the W from its decay products in both the $W^+W^- \rightarrow \ell\bar{\nu}_\ell q\bar{q}'$ and $W^+W^- \rightarrow q\bar{q}'\bar{q}q'$ channels. The W mass result for the 1998 data set is $M_W = 80.387 \pm 0.087(\text{stat}) \pm 0.034(\text{syst}) \pm 0.017(\text{LEP}) \pm 0.035(\text{FSI})$ GeV/c^2, where FSI represents the uncertainty due to final state interaction effects in the $q\bar{q}'\bar{q}q'$ channel, and LEP represents that arising from the knowledge of the beam energy of the accelerator. Combining this result with those previously published by the DELPHI Collaboration gives the result $M_W = 80.359 \pm 0.074(\text{stat}) \pm 0.032(\text{syst}) \pm 0.017(\text{LEP}) \pm 0.033(\text{FSI})$ GeV/c^2. The combined value for the W width is $\Gamma_W = 2.266 \pm 0.176(\text{stat}) \pm 0.056(\text{syst}) \pm 0.052(\text{FSI})$ GeV/c^2. © 2001 Elsevier Science B.V. All rights reserved.

---

[1] Now at DESY-Zeuthen, Platanenallee 6, D-15735 Zeuthen, Germany.

1. Introduction

The W mass has been measured by the DELPHI Collaboration using the data collected during 1998. This data sample has allowed a significant improvement in the accuracy of the collaboration's W mass determination as the integrated luminosity is more than twice that on which previous DELPHI results are based [1–3]. The W mass has also been determined by the other LEP Collaborations [4] and at hadron colliders [5]. Using the same reconstruction method as for the W mass, results on the direct measurement of the W width are also obtained in this Letter, and can be compared with those of the other LEP Collaborations and of the CDF Collaboration [6].

Section 2 of this Letter describes the characteristics of the 1998 data sample and of the event generators used in this analysis.

The analysis is performed through the direct reconstruction of the mass of the W from its decay products in the $W^+W^- \to q\bar{q}'\bar{q}q'$ (fully-hadronic) and $W^+W^- \to \ell\bar{\nu}_\ell q\bar{q}'$ (semi-leptonic) decay channels. The applied methods are described in Section 3, and have been refined from those in previous publications. Results are now reported for $\tau\bar{\nu}_\tau q\bar{q}'$ events, and in both the fully-hadronic and semi-leptonic channels improvements in the handling of initial-state radiation (ISR) have been included.

The systematic error evaluation described in Section 4 has increased in sophistication from that previously reported. New techniques have been applied, such as the use of mixed Lorentz boosted Z's, and a wider range of higher precision simulation studies have been performed.

The results of this analysis are reported in Section 5, and are combined with the previous DELPHI results.

2. Data and simulation samples

2.1. Data

A detailed description of the DELPHI apparatus and its performance can be found in [7].[2] In 1998 the detector was used to record data at the Z peak and at a nominal centre-of-mass energy of 189 GeV.

The Z peak data were recorded before (1.8 pb^{-1}) and towards the end (0.6 pb^{-1}) of the high energy data, thus facilitating checks of detector stability. These data were the principal sample used for calibration and alignment of the detector and, in this analysis, assist the study of systematic uncertainties.

The average centre-of-mass collision energy for the high energy data was 188.6 GeV. The luminosity weighted r.m.s. of this value, assessed on a fill by fill basis, was 50 MeV. In the data sample considered for analysis all the detectors essential for this measurement were required to be fully efficient; the operation of the central tracking detectors was important for all decay channels, in the $\ell\bar{\nu}_\ell q\bar{q}'$ analysis stricter requirements than in the $q\bar{q}'\bar{q}q'$ channel were placed on the electromagnetic calorimeters. The selected samples correspond to integrated luminosities of 152.9 pb^{-1} for the $\ell\bar{\nu}_\ell q\bar{q}'$ analysis and 157.4 pb^{-1} for the $q\bar{q}'\bar{q}q'$ decay channel.

2.2. Simulation

The response of the detector to various physical processes was modelled using the simulation program DELSIM [7], which includes modelling of the resolution, granularity and efficiency of the detector components. In addition, detector correction factors, described in Section 4, were included to improve the description of jets, electrons and muons. For systematic uncertainty studies a fast simulation program, relying on a relatively simple set of smearing and efficiency parametrisations, was also used.

WW events and all other four-fermion processes were produced using the event generator EXCALIBUR [8], with initial-state radiation described using the QEDPS program [9]. The W mass (M_W) and width (Γ_W) definition used throughout this Letter correspond to a W propagator with an s-dependent width. The background process $e^+e^- \to q\bar{q}(\gamma)$ was simulated with the PYTHIA 5.7 [10] event generator. Two photon backgrounds were studied using the TWOGAM generator [11]. The fragmentation of all events was performed using JETSET 7.4 [10] tuned to the DELPHI LEP1 data [12]. Systematic error checks were performed using other generators and variations in the fragmentation tuning as described in Section 4. The

---

[2] The coordinate system used has the z-axis parallel to the electron beam, and the polar angle calculated with respect to this axis.

systematics section also reports DELPHI results for the common LEP event samples produced in the context of the LEP WW workshops: the event generation was performed by ALEPH using KORALW 1.21 [13], and these events were then passed through the DEL-SIM program.

3. Analysis method

3.1. Semi-leptonic decay channel

The fitting procedure presented here is a development of that described in [3] for the $e\bar{\nu}_e q\bar{q}'$ and $\mu\bar{\nu}_\mu q\bar{q}'$ channels, where the fitting function now includes a description of the ISR spectrum of WW events. In addition, we present here an analysis of the $\tau\bar{\nu}_\tau q\bar{q}'$ channel and the event selection in all semi-leptonic channels is now based on a neural network.

3.1.1. Event selection

Lepton identification. Charged particles were identified as muons if they were associated with a hit in the muon chambers, or had an energy deposit in the hadron calorimeter that was consistent with a minimum ionising particle. Muon identification was performed in the polar angle range between $10°$ and $170°$.

Electron identification was performed in the polar angle range between $12°$ and $168°$ by selecting charged particles with a characteristic energy deposition in the electromagnetic calorimeters. In the central region of the detector covered by the HPC electromagnetic calorimeter, electrons were selected using the energy over momentum (E/p) ratio of the candidate. For lower energy candidates (below 30 GeV) this was supplemented by selection criteria on the shape of the calorimetric shower and a more stringent comparison of the track extrapolation and calorimetric shower positions, while for electrons of higher energy, negligible energy deposition in the hadron calorimeter was required. In the polar angle region below $36°$ and above $144°$, where the momentum resolution is poorer, tracks associated to electromagnetic energy showers above 8 GeV and negligible hadron calorimeter energy deposits were considered as electrons.

Tau candidates were obtained by clustering the events into a three-jet configuration using the LUCLUS

[14] algorithm. The jet with the lowest charged multiplicity was chosen as the tau candidate. As the tau lepton predominantly decays into a final state with one or three charged particles, only jets containing between one and four charged tracks were selected.

Selection. The event selection was based upon a multi-layer perceptron neural network [15]. The network was optimised separately for $e\bar{\nu}_e q\bar{q}'$, $\mu\bar{\nu}_\mu q\bar{q}'$, $\tau\bar{\nu}_\tau q\bar{q}'$ candidates containing only one charged particle and $\tau\bar{\nu}_\tau q\bar{q}'$ candidates with several charged particles.

Having removed the lepton candidate in $e\bar{\nu}_e q\bar{q}'$ and $\mu\bar{\nu}_\mu q\bar{q}'$ events, the LUCLUS jet clusterization algorithm (with a d_{join} of 7.5 GeV/c) was used to cluster the remaining particles. Events containing more than three jets were re-clustered, forcing them into a three-jet configuration. $\tau\bar{\nu}_\tau q\bar{q}'$ events were clustered as the tau candidate and a two-jet system. The events were reconstructed using a constrained fit imposing conservation of four-momentum and equality of the two W masses in the event. As the energy of the tau lepton is unknown, due to the emission of at least one neutrino in its decay, the mass in the $\tau\bar{\nu}_\tau q\bar{q}'$ channel is entirely determined by the jet system.

The neural network relied upon the characteristic event properties in each decay channel. The input variables included lepton momentum, polar angle of the missing momentum, and the isolation of the lepton candidate from the hadronic system of the event. The electron and muon identification was obtained as a strong or loose tag and the network was optimised separately in each decay channel for these two categories of identification.

The network was tuned on samples of signal and background simulation events, and its performance estimated on independent samples of events. After applying a cut on the network output the selection performance is as shown in Table 1. Events that passed the cut in the muon channel were selected, the remaining events were considered as electron channel candidates and, if they were again rejected, were then analysed under the tau channel hypothesis. The neural network output in the $\tau\bar{\nu}_\tau q\bar{q}'$ channel is shown in Fig. 1.

The tau selection sample contains a significant proportion of other semi-leptonic decays: the composition was estimated from simulation to be 67% $\tau\bar{\nu}_\tau q\bar{q}'$,

Table 1
Number of selected events from the 189 GeV data sample, and the corresponding number of expected events from the simulation. Column four is the sum of the three previous columns

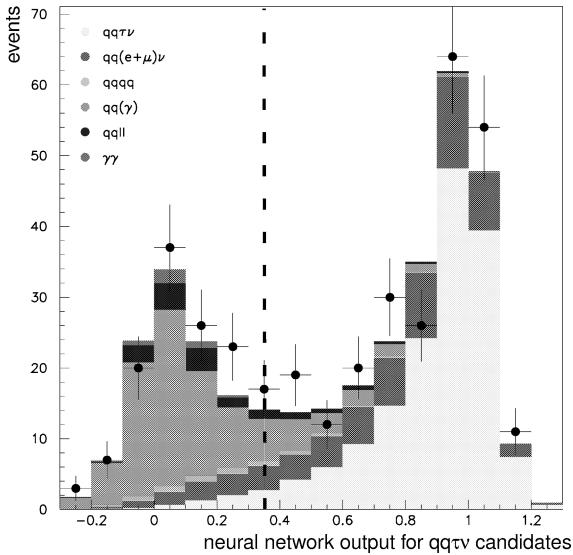| Event type	Event selection				
	$e\bar{\nu}_e q\bar{q}'$	$\mu\bar{\nu}_\mu q\bar{q}'$	$\tau\bar{\nu}_\tau q\bar{q}'$	$\ell\bar{\nu}_\ell q\bar{q}'$	$q\bar{q}'\bar{q}q'$
$e\bar{\nu}_e q\bar{q}'$	259.5	0.3	43.6	303.4	4.2
$\mu\bar{\nu}_\mu q\bar{q}'$	0.5	319.6	10.8	330.9	2.5
$\tau\bar{\nu}_\tau q\bar{q}'$	12.1	13.4	155.4	180.9	8.0
$q\bar{q}'\bar{q}q'$	0.2	0.2	1.7	2.1	1112.7
Other 4f	3.4	3.0	4.4	10.8	0.0
$q\bar{q}(\gamma)$ and other 2f	8.0	0.7	15.8	24.5	346.9
Total	283.7	337.2	231.7	852.6	1474.2
Data	244	307	236	787	1481

Fig. 1. The output distribution of the event selection neural network for $\tau\bar{\nu}_\tau q\bar{q}'$ candidates. The shaded areas indicate the contribution from the various simulated states, the data are shown as points with statistical error bars. The value of the selection cut applied is indicated by the dashed line. Note that the order of the simulation contributions in the figure follows that in the key, the $\tau\bar{\nu}_\tau q\bar{q}'$ signal is the first distribution shown and background from two-photon diagrams the last.

19% $e\bar{\nu}_e q\bar{q}'$, 5% $\mu\bar{\nu}_\mu q\bar{q}'$ with the remaining fraction dominated by $q\bar{q}(\gamma)$ background events. This corresponds to a 39% selection efficiency for $\tau\bar{\nu}_\tau q\bar{q}'$ events.

Further information on a selection of W^+W^- events in DELPHI with a similar performance is available in [16].

The fraction of semi-leptonic WW events in the sample was extracted from simulation as a function of the neural network output: this is referred to below as the event purity P_e. This feature is particularly useful for the tau selection, where the proportion of background events is highest.

3.1.2. Likelihood function

The following likelihood function was evaluated for each selected events with a reconstructed mass in the range 68–92 GeV/c^2:

$$\mathcal{L}_e(M_W, \Gamma_W) = P_e \cdot S''\left(m^{\text{fit}}, \sigma^{\text{fit}}, M_W, \Gamma_W\right) + (1 - P_e) \cdot B\left(m^{\text{fit}}\right), \quad (1)$$

where P_e is the event purity, discussed above, S'' is the signal function that describes the reconstructed mass distribution of the semi-leptonic W decays, and B is used to describe background processes. The reconstructed event mass m^{fit} and its estimated error σ^{fit} are both obtained from the constrained fit. The distribution of background events is extracted from simulation as a function of m^{fit}.

The signal function S'' is defined in terms of S, S' as discussed below. The function S relies on the convolution of three components, using x and m as the dummy integration variables:

$$S\left(m^{\text{fit}}, \sigma^{\text{fit}}, M_W, \Gamma_W\right)$$
$$= \int_0^{E_{\text{BEAM}}} dm\, G\left[m^{\text{fit}} - m, \sigma^{\text{fit}}\right]$$
$$\times \int_0^1 dx\, \text{BW}_{\text{PS}}\left[m \cdot (1 - x), M_W\, R_{\text{ISR}}(x)\right]. \quad (2)$$

BW_{PS} is a phase-space corrected relativistic Breit–Wigner distribution (representing the W mass distribution) which is convoluted with the Gaussian function G describing the detector resolution. The width of the Gaussian depends upon the reconstructed mass error obtained in the constrained fit for that event. Details of the BW_{PS} and G terms are given in [2]. A recent addition to the analysis is the description of the ISR

spectrum, which is parametrised as

$$R_{ISR}(x_\gamma) = \beta x_\gamma^{(\beta-1)}, \tag{3}$$

where x_γ is the ratio of the photon energy to the centre-of-mass energy and β is calculated from the electromagnetic constant (α), the centre-of-mass energy squared (s) and the electron mass (m_e):

$$\beta = \frac{2\alpha}{\pi}\left[\log(s/m_e^2) - 1\right]. \tag{4}$$

Including this ISR term decreases the bias on the fitted W mass by approximately 400 MeV and improves the expected error by $2 \pm 1\%$.

The event selection contains a significant fraction of $\tau\bar{\nu}_\tau q\bar{q}'$ events in the electron and muon channel samples, and of $e\bar{\nu}_e q\bar{q}'$ events in the tau sample (see Table 1). In the tau channel the mass of the event is determined from the jet system. The behaviour of true $\tau\bar{\nu}_\tau q\bar{q}'$ and $e\bar{\nu}_e q\bar{q}'$ events in this fit are found to be similar. However, in the electron and muon channel samples the behaviour of the $\tau\bar{\nu}_\tau q\bar{q}'$ events is somewhat different to that of the $e\bar{\nu}_e q\bar{q}'$, $\mu\bar{\nu}_\mu q\bar{q}'$ events. The $\tau\bar{\nu}_\tau q\bar{q}'$ events have a worse mass resolution and a small negative bias on the mass. The fraction of tau events, which have been wrongly classified and are contained in the electron and muon channel samples, has been parametrised in bins of the lepton energy and the measured missing mass. This event impurity $P\tau_e$ was then taken into account in the likelihood function for the electron and muon samples, by defining the signal function S'' as

$$S'' = (1 - P\tau_e) \cdot S + P\tau_e \cdot S', \tag{5}$$

where S' is analogous to S, but with the width of the Gaussian resolution function increased according to simulation studies. All remaining biases in the analysis due to using this approximate likelihood description are corrected for in the calibration procedure as described in Section 3.3.

3.2. Fully-hadronic decay channel

The analysis of the fully-hadronic channel was based on that applied in [3]. However, the implementation now relies on kinematic fits with four rather than six constraints and includes a new ISR treatment.

3.2.1. Event selection

A sample of hadronic events was selected by requiring more than 13 charged particles and a total visible energy exceeding 1.15 E_{BEAM}.

$q\bar{q}(\gamma)$ events were suppressed by demanding an effective centre-of-mass energy [17], after ISR emission, of greater than 161 GeV. The algorithm for assessing the e^+e^- collision energy considers both the emission of unobserved ISR photons in the beam-pipe and photon candidates detected in the electromagnetic calorimeters.

The DURHAM jet clustering algorithm [18] with y_{cut} of 0.002 was applied to the event. If any of the resulting jets contained less than three particles or had an invariant mass smaller than 1 GeV/c^2, clustering was continued to a higher value of y_{cut}. Events with less than four jets were then rejected, while events containing six or more jets were re-clustered into five objects representing four quarks plus one hard gluon jet.

Events containing b-quarks were rejected using the DELPHI b-tag package [19], this removes 17% of ZZ events and 6% of $q\bar{q}(\gamma)$ background while reducing the signal efficiency by only 0.2%. A four constrained kinematic fit [3] was applied to the remaining events, enforcing conservation of energy and momentum.

A variable to discriminate between $q\bar{q}$ events with hard gluon radiation and signal events was constructed. This compound variable relied upon the fitted jet energies and the inter-jet angles. The expected fraction of $q\bar{q}'\bar{q}q'$ events in the selected sample, the event purity, was parametrised as a function of this variable. Events with an estimated purity below 25% were rejected.

The performance of the event selection is shown in Table 1. Further information on a selection of W^+W^- events in DELPHI with a similar performance is available in [16].

3.2.2. Likelihood function

For each of the selected events an event likelihood was constructed:

$$\mathcal{L}_e(M_W, \Gamma_W) = \iint \sum_i w_{i,e}\, p_{i,e}(m_x, m_y)$$
$$\times \left[P_e^{eff} S(m_x, m_y, M_W, \Gamma_W)\right.$$
$$\left. + (1 - P_e^{eff}) \cdot B\right] dm_x\, dm_y. \tag{6}$$

As in [3] the signal function $S(m_x, m_y, M_W, \Gamma_W)$ consists of Breit–Wigner terms for the WW and the ZZ contribution and a phase space correction factor. A flat distribution B accounts for background processes and wrong jet pairings in the signal events. Both S and B were normalised to 1 over the integration area. The fraction of the signal and background likelihoods used for each event depend upon the event purity P_e^{eff}. This purity was parametrised as a function of a discriminating variable as described above.

The sum $\sum_i w_{i,e} p_{i,e}(m_x, m_y)$ is a weighted sum of the probability densities $p_{i,e}$ that the event e corresponds to two heavy objects with mass m_x and m_y.

The probability density

$$p_{i,e}(m_x, m_y) \propto \exp\left[-\tfrac{1}{2}\chi^2_{i,e}(m_x, m_y)\right]$$

was determined for all jet pairings (three possibilities for a four-jet event and ten for a five-jet event) and with three different clustering algorithms (DURHAM [18], CAMJET [20] and DICLUS [21]). The relative probabilities $w_{i,e}$ that the corresponding jet pairing was the correct one were estimated using jet charge information and the transverse momentum of the gluon candidate (see [3]). The three jet clustering algorithms were given the same weight.

The probability was calculated using a Gaussian approximation for the χ^2:

$$\chi^2_{i,e}(m_x, m_y) \approx \chi^2_{4C} + \left(\mathbf{m} - \mathbf{m}^{\text{fit}}\right)^T \mathbf{V}^{-1}\left(\mathbf{m} - \mathbf{m}^{\text{fit}}\right) \quad (7)$$

with

$$\mathbf{V} = \begin{pmatrix} \sigma^2_{m_x} & \sigma_{m_x}\sigma_{m_y}\rho_{xy} \\ \sigma_{m_x}\sigma_{m_y}\rho_{xy} & \sigma^2_{m_y} \end{pmatrix},$$
$$\mathbf{m} = \begin{pmatrix} m_x \\ m_y \end{pmatrix} \quad \text{and} \quad \mathbf{m}^{\text{fit}} = \begin{pmatrix} m_x^{\text{fit}} \\ m_y^{\text{fit}} \end{pmatrix}.$$

The masses m_x^{fit}, m_y^{fit}, their errors σ_{m_x} and σ_{m_y} and the correlation between them, ρ_{xy}, are taken from a four constrained kinematic fit. When the χ^2_{4C} is larger than the number of degrees of freedom (NDF = 4), the $\chi^2_{i,e}(m_x, m_y)$ is rescaled with a factor NDF$/\chi^2_{4C}$ in order to compensate for non-Gaussian resolution effects. This procedure decreases the computing time taken by an order of magnitude compared with the full six constrained fit [3], while resulting in only a minimal reduction in the W mass precision obtained ($2 \pm 1\%$).

A new feature of this analysis is a treatment of events under the collinear ISR hypothesis. A kinematic fit was performed with modified constraints to simulate the emission of an ISR photon of momentum p_z inside the beam pipe:

$$\sum_{i=1}^{n_{\text{objects}}} (E, p_x, p_y, p_z)_i = \left(\sqrt{s} - \left|p_z^{\text{fit}}\right|, 0, 0, p_z^{\text{fit}}\right). \quad (8)$$

The probability that the missing momentum in the z direction was indeed due to an unseen ISR photon was extracted from the simulation as a function of $|p_z^{\text{fit}}|/\sigma_{p_z}$, where σ_{p_z} is the estimated error on the fitted z momentum component; only events with this ratio greater than 1.5 were treated with the mechanism described below.

Additional probability density $p_{i,e}$ terms were then included in the likelihood sum for these events, with a relative weight factor derived from the ISR hypothesis probability. An example of the effect of including the ISR hypothesis is shown in Fig. 2. This treatment was applied to 16% of the events and resulted in an improvement of the expected W mass error for these events of 15%.

3.3. Mass and width extraction

The distribution of the reconstructed invariant masses of the selected events after applying a kinematic fit, imposing four-momentum conservation and the equality of the two di-jet masses, are shown in Fig. 3. This plot is provided for illustrative purposes only, the mass and width fitting procedure is described below.

The combined likelihood of the data can be obtained from the product of the event likelihoods described above. The W mass and width were extracted from maximum likelihood fits. The W mass fit is performed assuming the standard model value for the W width. The W width was obtained assuming a mass of 80.35 GeV/c^2. The correlation between M_W and Γ_W was found to have a negligible impact on the extracted width value.

The mass and width analyses have been calibrated separately in each of the decay channels ($q\bar{q}'\bar{q}q'$, $e\bar{\nu}_e q\bar{q}'$, $\mu\bar{\nu}_\mu q\bar{q}'$, $\tau\bar{\nu}_\tau q\bar{q}'$). The biases of the analyses were estimated by re-weighting generated simulation samples to obtain the fitted mass and width values. The re-weighting was performed using the extracted
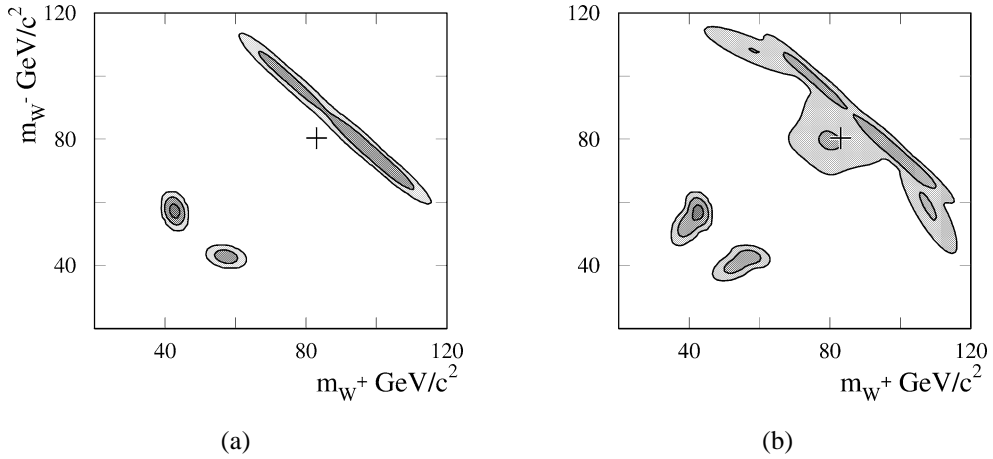
Fig. 2. An example of the reconstructed probability density function $\sum_i w_{i,e} p_{i,e}(m_+, m_-)$ (see text) for the invariant masses in a simulated 4-jet $q\bar{q}'\bar{q}q'$ event without (a) and with (b) the hypothesis of collinear ISR. The first 3 sigma contours are shown. The normalization of the different solutions prevents the high mass contours from reaching the 1 sigma probability level, while the small difference in the low mass solutions originates from the jet charge information. The generated masses of the two W bosons in the event are marked with a cross.

matrix element of the EXCALIBUR generator. The linearity of the mass analysis was estimated using independent simulation samples generated at three W mass values, while the re-weighting procedure was used for the width analysis. The analyses were corrected with the calibration results, and the statistical error on the bias is included in the systematic error.

The analyses were checked by performing fits to a large number of samples of simulation events. Each sample was comprised of a mixture of signal and background simulation events to represent the expected distribution in the data. The pull distribution $(m_{\text{fit}} - m_{\text{W}})/\sigma_{\text{fit}}$ was demonstrated to be compatible with a Gaussian of width one to an accuracy of better than 1%. The mean expected statistical error in the W mass was 262 MeV/c^2 for e$\bar{\nu}_e$q$\bar{q}'$, 203 MeV/c^2 for $\mu\bar{\nu}_\mu$q$\bar{q}'$, 311 MeV/c^2 for $\tau\bar{\nu}_\tau$q$\bar{q}'$ and 104 MeV/c^2 for the q$\bar{q}'\bar{q}q'$ channel.

4. Systematic uncertainties

The sources of systematic error that have been considered for the W mass and width determinations are described in the subsections below. The results of these studies are summarised in Tables 8 and 9.

4.1. Calibration

The accuracy with which the bias of the analysis can be determined is limited by the size of the generated simulation samples. Sufficient events were generated to limit this error to less than 10% of the statistical error in any given channel. The calibration procedure is described in Section 3.3.

4.2. Detector effects

The data taken at the Z peak were used to study, and limit, possible errors in the detector simulation model.

Muon studies were performed on a selected sample of Z $\rightarrow \mu^+\mu^-$ events. From the di-muon sample corrections to the inverse momentum scale, $1/p$, were calculated separately for positive and negative muons as a function of the lepton polar angle. The systematic error on this correction was estimated by varying it by half of its value. The momentum resolution (typically 0.001 in $1/p$) was found to be slightly better in simulation than in the data (a maximum difference of 10%). This was corrected by smearing the simulation with a Gaussian. An extra smearing of 0.0005 in $1/p$ was used to estimate the systematic error coming from this correction. The combined systematic error from these corrections is quoted for the $\mu\bar{\nu}_\mu$q$\bar{q}'$ channel
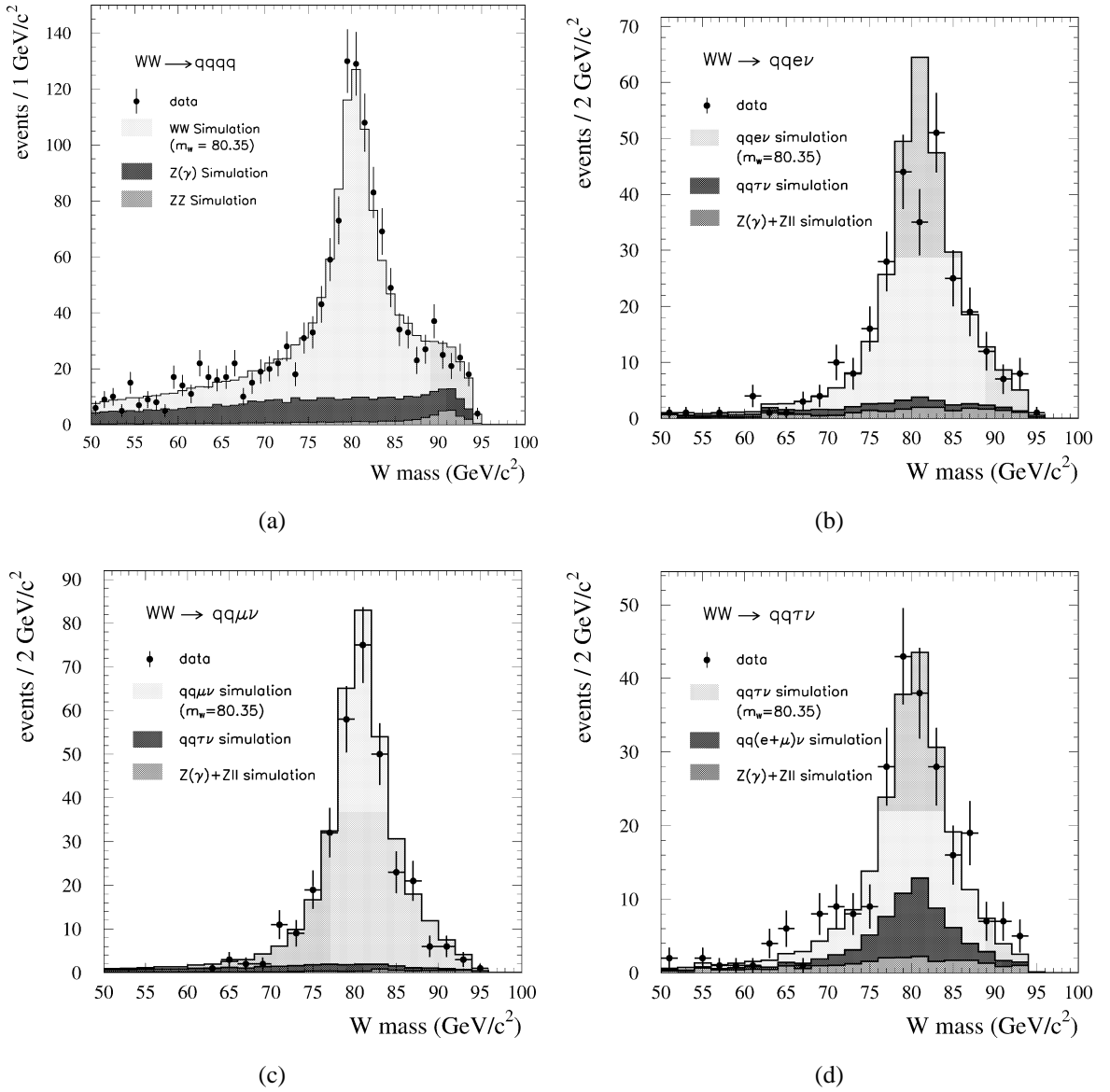
Fig. 3. The distribution of the reconstructed W masses from a kinematic fit with five constraints imposed in the (a) $q\bar{q}'\bar{q}q'$, (b) $e\bar{\nu}_e q\bar{q}'$, (c) $\mu\bar{\nu}_\mu q\bar{q}'$ and (d) $\tau\bar{\nu}_\tau q\bar{q}'$ analysis channels. In the $q\bar{q}'\bar{q}q'$ channel, only the jet pairing with the highest probability is included in this figure.

as the lepton correction systematic error in Tables 8 and 9.

The correction of the energy scale of electrons was determined from Bhabha events at the Z peak in different polar angle regions. The residual systematic error on this absolute energy scale was estimated to be 0.5%. In each of these polar angle regions, the energy resolution of simulation events was degraded by applying a Gaussian smearing, and the residual error on this smearing was estimated to be 1%. The dependence of the energy calibration as a function of the electron energy was checked using low energy

electrons from Compton events at the Z peak, and high energy electrons from radiative Bhabha scattering at high centre-of-mass energy. In these cases the true energy of the lepton was deduced from 3-body kinematics using only the angular information and assuming that the unseen particle was along the beam axis. The absolute energy calibration was found to be compatible with requiring no additional corrections in all energy ranges. The systematic error coming from this source was estimated assuming a 1% change of slope in the energy calibration in the range of interest (between 25 and 70 GeV). The lepton correction uncertainty for the $e\bar{\nu}_e q\bar{q}'$ channel, quoted in Tables 8 and 9, is the quadratic sum of the errors from these three error sources.

The lepton correction error is not quoted for the $\tau\bar{\nu}_\tau q\bar{q}'$ channel as the reconstructed tau lepton carries no information for the reconstructed W mass.

Jet energies were studied in $Z \rightarrow q\bar{q}$ events as a function of the polar angle and reconstructed energy of the jet. The comparison of data and simulation showed agreement within a band of $\pm 2\%$ over most of the DELPHI detector's angular coverage and an overall uncertainty of 1% was estimated. The simulation was smeared by a Gaussian function to improve the description of the observed energy spread in the data and the residual error on this smearing was estimated to be $\pm 4\%$. The dependence of the energy calibration as a function of the jet energy was checked using low energy jets from $q\bar{q}$ + gluon events at the Z peak and high energy jets from radiative Z's at high centre-of-mass energy. The true jet energy was estimated from 3-body kinematics; in the radiative events the unseen photon was assumed to be along the beam axis. No additional energy calibration slope was necessary over the relevant energy range (25 to 75 GeV) and a 1% change in slope was used to calculate the systematic error. A study of the acollinearity of jets in $Z \rightarrow q\bar{q}$ events was performed and an appropriate smearing to the simulation of the jet angular direction was estimated. A systematic error was estimated by applying an extra 5 mrad angular smearing. The jet correction uncertainty, quoted in Tables 8 and 9, is the quadratic sum of these four errors.

A possible source of angular distortion in DELPHI is the uncertainty on the length to width ratio of the detector. The detector is aligned relative to the vertex detector, the largest uncertainty being the radius of this detector which is known to a precision of $\pm 0.1\%$. This error is listed in the M_W systematics table under aspect ratio. The corresponding uncertainty for the width measurement is less than 10 MeV.

4.3. Background description

The background level was changed by $\pm 10\%$ in the simulation; this easily covers the expected uncertainty in the accepted cross-section, as discussed in [16]. The dominant background source, $Z \rightarrow q\bar{q}(\gamma)$, was generated using both JETSET and HERWIG fragmentation models and mass fits performed using both these samples. The 4-jet rate in data and simulation was also studied using events collected at the Z peak. It is concluded that the background description is a relatively small component of the systematic error for the mass measurement, as shown in Table 8 and somewhat more important for the width (see Table 9).

4.4. Fragmentation

A study of the possible effects on M_W and Γ_W of the simulation of the event fragmentation was performed, the results are provided in Tables 2 and 3.

Events were produced using a fast simulation package where the value of Λ_{QCD} and σ_q were changed with respect to the standard DELPHI JETSET tuned values [12] by twice their estimated errors.[3] The estimated errors are ± 0.018 GeV for Λ_{QCD} and ± 0.007 GeV for σ_q.

The event samples generated by ALEPH in the context of the LEP WW workshop are used to compare results from the HERWIG and JETSET fragmentation models. The HERWIG events were produced with a recent tuning [22] which provides a better description of the data than previous HERWIG versions.

The results on the DELPHI tuning of JETSET are also compared with those of the ALEPH Collaboration. This comparison cross-checks several effects as the ALEPH events were produced with a different generator (KORALW) from the DELPHI events which includes a different ISR and final-state radiation (FSR) treatment.

---

[3] The dominant systematic error components of the tuning uncertainties were estimated from a comparison of fits with a range of input data distributions.

Table 2

Results of a study of fragmentation effects on the M_W measurement (see text). All results are given for the fitted mass analyses on the samples studied with respect to the standard DELPHI JETSET sample, unless otherwise stated. The statistical error on the observed difference is also given

	M_W fragmentation study (MeV/c^2)			
Event type	$e\bar{\nu}_e q\bar{q}'$	$\mu\bar{\nu}_\mu q\bar{q}'$	$\tau\bar{\nu}_\tau q\bar{q}'$	$q\bar{q}'\bar{q}q'$
$\Lambda_{QCD} - 2\sigma$	0 ± 14	$+9 \pm 16$	$+30 \pm 30$	$+3 \pm 6$
$\Lambda_{QCD} + 2\sigma$	-4 ± 14	$+10 \pm 16$	-10 ± 30	-7 ± 6
$\sigma_q - 2\sigma$	0 ± 14	$+30 \pm 16$	-3 ± 30	-9 ± 6
$\sigma_q + 2\sigma$	0 ± 14	$+30 \pm 16$	$+27 \pm 30$	-3 ± 6
ALEPH HERWIG – ALEPH JETSET	75 ± 52	8 ± 42	106 ± 66	-6 ± 18
ALEPH JETSET	15 ± 51	-17 ± 42	-81 ± 65	$+3 \pm 18$

Table 3

Results of a study of fragmentation effects on the Γ_W measurement (see text). All results are given for the fitted mass analyses on the samples studied with respect to the standard DELPHI JETSET sample, unless otherwise stated. The statistical error on the observed difference is also given

	Γ_W fragmentation study (MeV/c^2)			
Event type	$e\bar{\nu}_e q\bar{q}'$	$\mu\bar{\nu}_\mu q\bar{q}'$	$\tau\bar{\nu}_\tau q\bar{q}'$	$q\bar{q}'\bar{q}q'$
$\Lambda_{QCD} - 2\sigma$	-5 ± 30	-46 ± 35	-8 ± 59	-4 ± 12
$\Lambda_{QCD} + 2\sigma$	$+11 \pm 30$	-47 ± 35	$+57 \pm 59$	$+15 \pm 12$
$\sigma_q - 2\sigma$	$+16 \pm 30$	-76 ± 35	-11 ± 59	-11 ± 12
$\sigma_q + 2\sigma$	$+28 \pm 30$	-78 ± 35	-30 ± 59	-2 ± 12
ALEPH HERWIG – ALEPH JETSET	-148 ± 113	-47 ± 95	-155 ± 158	-68 ± 38
ALEPH JETSET	$+264 \pm 108$	-30 ± 95	$+176 \pm 157$	$+4 \pm 43$

As the results in Tables 2 and 3 are all compatible with zero, we quote a systematic error from fragmentation reflecting twice the statistical precision of the JETSET tuning parameter studies in the combined semi-leptonic and fully-hadronic channels.

4.5. Mixed Lorentz boosted Z's

The agreement between data and simulation can be cross-checked using the method of mixed Lorentz boosted Z's. Z events were selected from the Z peak data sample collected during 1998 and the corresponding simulation sample. Through a suitable choice of Lorentz boost and superimposing two Z events a WW event may be emulated. The angular distribution of the Z events used was chosen to match that expected in WW events.

This technique has been applied to the $q\bar{q}'\bar{q}q'$ mass measurement and the hadronic system in semi-leptonic events. The differences between data and simulation obtained are 2 ± 2 MeV/c^2 and 3 ± 10 MeV/c^2 in the two topologies respectively, where the errors are statistical. These results reinforce the view that the quoted systematic errors for detector and fragmentation effects are conservative. A study of possible intrinsic uncertainties of the MLBZ method [23] in the $q\bar{q}'\bar{q}q'$ channel estimates the accuracy of this technique to be 5 MeV/c^2, and demonstrates excellent agreement between data and simulation as a function of relevant event variables.

Table 4
A comparison of two ISR treatments for the M_W measurement, the KORALW form and the QEDPS treatment. The statistical error on the result is also provided

	M_W ISR study (MeV/c^2)			
Model	$e\bar{\nu}_e q\bar{q}'$	$\mu\bar{\nu}_\mu q\bar{q}'$	$\tau\bar{\nu}_\tau q\bar{q}'$	$q\bar{q}'\bar{q}q'$
KORALW re-weighted – QEDPS	$+2 \pm 7$	0 ± 5	-12 ± 8	-16 ± 3

Table 5
A comparison of two ISR treatments for the Γ_W measurement, the KORALW form and the QEDPS treatment. The statistical error on the result is also provided

	Γ_W ISR study (MeV/c^2)			
Model	$e\bar{\nu}_e q\bar{q}'$	$\mu\bar{\nu}_\mu q\bar{q}'$	$\tau\bar{\nu}_\tau q\bar{q}'$	$q\bar{q}'\bar{q}q'$
KORALW re-weighted – QEDPS	$+13 \pm 13$	$+14 \pm 10$	$+4 \pm 16$	-16 ± 5

4.6. ISR

A comparison of two independent models of ISR was performed. WW events produced with the EX-CALIBUR generator were re-weighted as a function of the total ISR energy in the event. The weights were obtained for each WW decay channel from a generator level study of the KORALW [13] ISR treatment (based on the YFS exponentiation approach) and that of the standard algorithm used in DELPHI QEDPS [9] (based on a parton shower approach). The results of the W mass and width fits are shown in Tables 4 and 5. We conservatively choose to quote the largest deviation observed in any of the channels.

4.7. LEP beam energy

The average LEP beam energy at DELPHI is evaluated by the energy working group [24] at 15 minute intervals of running or after significant changes in the beam energy. The measured centre-of-mass energy is imposed as a constraint in the kinematic fit, and hence the relative error on the beam energy translates to the same fractional error on the W mass determination. The spread of energies of the electrons and positrons in the LEP beams was found to have a negligible impact on the mass and width measurements.

4.8. Bose–Einstein correlations

Bose–Einstein statistics dictate that the production amplitude for final state particles should be symmetrical under the exchange of identical bosons. The omission of these correlations between particles from different W bosons in our standard simulation could lead to a systematic error on the W mass and width measurement in the $q\bar{q}'\bar{q}q'$ channel. A clear picture has yet to emerge from the experimental study of this phenomenon [25].

To evaluate the possible size of the effect on the mass and width measurements we have considered several phenomenological models; the results are given in Table 6. The relevant value for the systematic uncertainty is the difference between the shifts obtained from Bose–Einstein correlations inside individual W's and that between W's. The models used are:

- The LUBOEI algorithm [26] in JETSET changes the momentum vectors of identical final state bosons to model the two particle correlation function, and then offers a range of options to restore energy and momentum conservation.
- Global re-weighting aims to reproduce the enhancement of identical bosons close in phase-space by giving weights to events. This procedure does ensure energy and momentum conservation, but may adversely affect other event distributions. DELPHI results were obtained using the Kartvel-

Table 6
Results of the DELPHI studies on Bose–Einstein correlations, see text for details. The BE_{32} samples were produced with $\lambda = 1.35$, $r = 0.6$ fm

Bose–Einstein correlations study (MeV/c^2)		
Model	M_W shift	Γ_W shift
KKM model (183 GeV)	-10 ± 10	–
ST model BE (183 GeV) inside W's – none	$+0 \pm 10$	–
ST model BE (183 GeV) between W's – inside W's	$+3 \pm 11$	–
LUBOEI BE_{32} (189 GeV) inside W's – none	$+18 \pm 5$	$+13 \pm 11$
LUBOEI BE_{32} (189 GeV) between W's – inside W's	-32 ± 4	$+26 \pm 8$

ishvili/Kvatadze/Møller (KKM) re-weighting scheme [27] and reported on in [3].

- In [3] we also reported results for a study based on a modification of the JETSET fragmentation model introducing quantum mechanical 2-particle and 3-particle interference (ST) for identical bosons using a local re-weighting technique [28].

The version of LUBOEI model studied here is BE_{32}, in which a local energy and momentum conservation procedure is applied [26]. Six sets of fully simulated Z events were generated at a range of values of correlation strength (λ) and radius (r), and the four momentum difference, Q, between all selected same charge particle pairs was calculated. An interpolation was performed on the basis of the Q distribution to obtain $\lambda = 1.35$ and $r = 0.6$ fm (PARJ(93) = 0.34 GeV) which provide the optimal description of the DELPHI Z peak data. The simulated event samples were produced with the standard DELPHI JETSET tuning. The W mass and width shifts were evaluated using samples produced with fast simulation.

4.9. Colour reconnection

The hadronization of two W bosons in the $q\bar{q}'\bar{q}q'$ channel may not occur independently. The colour flow between the W's may lead to a shift in the measured W mass. Although experimental work is progressing [29], a suitable sensitivity has not yet been reached by the measurements to limit the effect on M_W.

In the previous publication [3] we reported results with the ARIADNE colour reconnection model, the results are repeated in Table 7. However, we note that the current version of the ARIADNE 2 model is dis-

Table 7
Results of the DELPHI studies on colour reconnection effects, see text for details. For the SK1 model results are given for 30% of reconnected events

Colour reconnection study (MeV/c^2)		
Model	M_W shift	Γ_W shift
ARIADNE CR 2 (183 GeV)	$+28 \pm 6$	–
ARIADNE CR 3 (183 GeV)	$+55 \pm 6$	–
JETSET SK1	46 ± 2	54 ± 3
JETSET SK1 improved sampling	44 ± 2	32 ± 3
JETSET SK2	-2 ± 5	37 ± 10

favoured by LEP1 data [30], and that we do not consider the ARIADNE 3 model for the systematic error assessment as it allows perturbative phase reconnection where calculations have shown the effect to be small [31].

The Sjöstrand/Khoze models of colour reconnection are available in the JETSET frame-work. We have used the SK1 and SK2 models. Results for the SK1 model are quoted for 30% of reconnected events, this is the same reconnected fraction as in the SK2 model. Events were produced using DELSIM and a fast detector simulation. By processing the same event sample through the full detector simulation and the fast simulation, the reliability of the fast detector simulation for this study was clearly demonstrated. The simulated event samples were produced with the standard DELPHI JETSET tuning.

However, we report that the standard implementation of SK1 shows numerical instabilities that reduce the reliability of the model used. In this model the re-
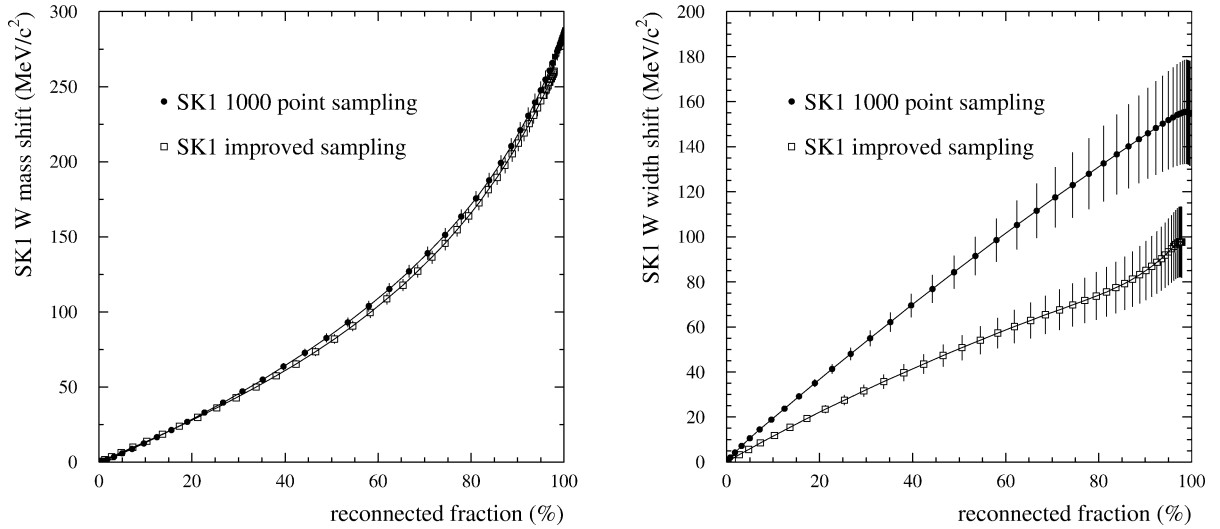
Fig. 4. Observed shift in the fitted mass (left) and width (right) as a function of the fraction of reconnected events, using the SK1 implementations as described in the text.

Table 8
Contributions to the systematic error on the W mass measurement

Sources of systematic error	M_W systematic errors (MeV/c^2)				
	$e\bar{\nu}_e q\bar{q}'$	$\mu\bar{\nu}_\mu q\bar{q}'$	$\tau\bar{\nu}_\tau q\bar{q}'$	$\ell\bar{\nu}_\ell q\bar{q}'$	$q\bar{q}'\bar{q}q'$
Statistical error on calibration	18	15	23	10	7
Lepton corrections	29	11	–	10	–
Jet corrections	39	27	48	35	18
Aspect ratio	2	2	2	2	4
Background	10	3	4	3	5
Fragmentation	20	20	20	20	12
ISR	16	16	16	16	16
LEP energy	17	17	17	17	17
Colour reconnection	–	–	–	–	46
Bose–Einstein correlations	–	–	–	–	32

connection probability is a function of the string overlap. This overlap is calculated by numerical integration through sampling. The accuracy of this calculation is improved by using 1000 sampling points rather than the default value of 100. In addition, we also report results from a more efficient sampling of the string overlap, in which the sampling is performed along strings taking into account their life-time and the total overlap is calculated as the sum of the overlap of pairs of string pieces.

The observed W mass and width shifts are given in Table 7 and in Fig. 4 the observed W mass and width shifts are shown as functions of the reconnected fraction of events in the SK1 model.

We conservatively choose to quote as a systematic error the largest effect observed in our studies; this is

Table 9
Contributions to the systematic error on the W width measurement

Sources of systematic error	Γ_W systematic errors (MeV/c^2)				
	$e\bar{\nu}_e q\bar{q}'$	$\mu\bar{\nu}_\mu q\bar{q}'$	$\tau\bar{\nu}_\tau q\bar{q}'$	$\ell\bar{\nu}_\ell q\bar{q}'$	$q\bar{q}'\bar{q}q'$
Statistical error on calibration	45	37	56	26	17
Lepton corrections	41	46	–	28	–
Jet corrections	82	43	102	63	26
Background	29	8	82	19	40
Fragmentation	42	42	42	42	24
ISR	16	16	16	16	16
Colour reconnection	–	–	–	–	54
Bose–Einstein correlations	–	–	–	–	26

approximately 50 MeV for both the mass and width analyses.

4.10. Correlations

The components of the systematic error arising from the jet energy scale corrections, aspect ratio, ISR, fragmentation and LEP beam energy are taken as correlated between the analyses in the different decay channels for the 189 GeV data. The background description and lepton modelling uncertainties are treated as uncorrelated between WW decay channels.

In Section 5.2 a combination with the previously published DELPHI results is performed. The LEP energy correlation matrix is used [24] in this process. The calibration statistics error is uncorrelated between years, while all other systematic errors are conservatively assumed to be fully correlated between years.

5. Results

5.1. 189 GeV results

The W mass and width results of the analyses described in this Letter are presented in Tables 10 and 11. The error is divided into its statistical component, indicated (stat), the main systematic component (syst) and the systematic from the beam energy uncertainty

(LEP). In the $q\bar{q}'\bar{q}q'$ channel an error from final state interaction effects (FSI) is also included.

The semi-leptonic and fully-hadronic W mass results are combined and the following result obtained:

$$M_W = 80.387 \pm 0.087(\text{stat}) \pm 0.034(\text{syst})$$
$$\pm 0.017(\text{LEP}) \pm 0.035(\text{FSI}) \text{ GeV}/c^2.$$

The combined result for the W width is:

$$\Gamma_W = 2.205 \pm 0.195(\text{stat}) \pm 0.059(\text{syst})$$
$$\pm 0.047(\text{FSI}) \text{ GeV}/c^2.$$

5.2. Combined DELPHI results

These results are combined with the previously published DELPHI results on the W mass determination by direct reconstruction [2,3] and the result from the threshold cross-section measurement [1] to obtain:

$$M_W = 80.359 \pm 0.074(\text{stat}) \pm 0.032(\text{syst})$$
$$\pm 0.017(\text{LEP}) \pm 0.033(\text{FSI}) \text{ GeV}/c^2.$$

This combination has a χ^2 of 4.5 with 6 degrees of freedom. The combined result on the W mass from the $q\bar{q}'\bar{q}q'$ channel alone is:

$$M_W = 80.369 \pm 0.091(\text{stat}) \pm 0.029(\text{syst})$$
$$\pm 0.017(\text{LEP}) \pm 0.056(\text{FSI}) \text{ GeV}/c^2$$

Table 10
189 GeV M_W results. The error is divided into its statistical component, indicated stat, the main systematic component syst and the systematic from the beam energy uncertainty LEP. In the $q\bar{q}'\bar{q}q'$ channel an error from final state interaction effects FSI is also included. The $\ell\bar{\nu}_\ell q\bar{q}'$ results represents the combination of the results obtained in the three semi-leptonic channels

189 GeV M_W results (GeV/c^2)				
Channel	M_W	stat	syst	LEP	FSI
$e\bar{\nu}_e q\bar{q}'$	80.478	±0.291	±0.059	±0.017	–
$\mu\bar{\nu}_\mu q\bar{q}'$	80.195	±0.213	±0.042	±0.017	–
$\tau\bar{\nu}_\tau q\bar{q}'$	80.114	±0.319	±0.059	±0.017	–
$\ell\bar{\nu}_\ell q\bar{q}'$	80.253	±0.151	±0.046	±0.017	–
$q\bar{q}'\bar{q}q'$	80.466	±0.106	±0.028	±0.017	±0.056

Table 11
189 GeV Γ_W results. The error is divided into its statistical component, indicated stat, the main systematic component syst and the systematic from the beam energy uncertainty LEP. In the $q\bar{q}'\bar{q}q'$ channel an error from final state interaction effects FSI is also included. The $\ell\bar{\nu}_\ell q\bar{q}'$ results represents the combination of the results obtained in the three semi-leptonic channels

189 GeV Γ_W results (GeV/c^2)				
Channel	Γ_W	stat	syst	FSI
$e\bar{\nu}_e q\bar{q}'$	4.358	±0.956	±0.115	–
$\mu\bar{\nu}_\mu q\bar{q}'$	2.353	±0.552	±0.086	–
$\tau\bar{\nu}_\tau q\bar{q}'$	2.799	±0.927	±0.149	–
$\ell\bar{\nu}_\ell q\bar{q}'$	2.842	±0.425	±0.088	–
$q\bar{q}'\bar{q}q'$	2.025	±0.220	±0.058	±0.060

and for the $\ell\bar{\nu}_\ell q\bar{q}'$ channel alone is:

$$M_W = 80.327 \pm 0.128(\text{stat}) \pm 0.045(\text{syst})$$
$$\pm 0.017(\text{LEP}) \text{ GeV}/c^2.$$

The mass difference between the measurements for the fully-hadronic and semi-leptonic channels, $\Delta M_W(q\bar{q}'\bar{q}q' - \ell\bar{\nu}_\ell q\bar{q}')$, has been determined:

$$\Delta M_W(q\bar{q}'\bar{q}q' - \ell\bar{\nu}_\ell q\bar{q}') = 39 \pm 159 \text{ MeV}/c^2.$$

A significant non-zero value for ΔM_W could indicate that FSI effects are biasing the value of M_W determined from the $q\bar{q}'\bar{q}q'$ events. As ΔM_W is primarily of interest as a check of the possible effects of final state interactions, the errors from FSI effects are set to zero in this determination: all other errors and correlations were as described above.

The combination for the W width with the 1997 data [3] yields:

$$\Gamma_W = 2.266 \pm 0.176(\text{stat}) \pm 0.056(\text{syst})$$
$$\pm 0.052(\text{FSI}) \text{ GeV}/c^2.$$

Acknowledgements

References

[1] DELPHI Collaboration, P. Abreu et al., Phys. Lett. B 397 (1997) 158.

[2] DELPHI Collaboration, P. Abreu et al., Eur. Phys. J. C 2 (1998) 581.

[3] DELPHI Collaboration, P. Abreu et al., Phys. Lett. B 462 (1999) 410.

[4] ALEPH Collaboration, R. Barate et al., Eur. Phys. J. C 17 (2000) 241;
L3 Collaboration, M. Acciarri et al., Phys. Lett. B 454 (1999) 386;
OPAL Collaboration, G. Abbiendi et al., hep-ex/0009018.

[5] CDF Collaboration, T. Affolder et al., hep-ex/0007044, to be published in Phys. Rev. D;
D0 Collaboration, B. Abbott et al., Phys. Rev. Lett. 80 (1998) 3008;
D0 Collaboration, B. Abbott et al., Phys. Rev. Lett. 84 (2000) 222.

[6] CDF Collaboration, T. Affolder et al., Phys. Rev. Lett. 85 (2000) 3347.

[7] DELPHI Collaboration, P. Aarnio et al., Nucl. Instrum. Methods A 303 (1991) 233;
DELPHI Collaboration, P. Abreu et al., Nucl. Instrum. Methods A 378 (1996) 57.

[8] F.A. Berends, R. Pittau, R. Kleiss, Comp. Phys. Commun. 85 (1995) 437.

[9] Y. Kurihara, J. Fujimoto, T. Munehisha, Y. Shimizu, Prog. Theor. Phys. 96 (1996) 1223.

[10] T. Sjöstrand, Comp. Phys. Commun. 82 (1994) 74.

[11] S. Nova, A. Olchevski, T. Todorov, in: Physics at LEP2, CERN 96-01, Vol. 2, 1996, p. 224.

[12] DELPHI Collaboration, P. Abreu et al., Z. Phys. C 73 (1996) 11.

[13] S. Jadach, W. Placzek, M. Skrzypek, B.F.L. Ward, Z. Was, Comp. Phys. Commun. 119 (1999) 272.

[14] T. Sjöstrand, PYTHIA 5.7 and JETSET 7.4: Physics and Manual, CERN-TH-7112-93-REV, 1995.

[15] Code kindly provided by J. Schwindling and B. Mansoulie.

[16] DELPHI Collaboration, P. Abreu et al., Phys. Lett. B 479 (2000) 89.

[17] P. Abreu et al., Nucl. Instrum. Methods A 427 (1999) 487.

[18] S. Catani, Yu.L. Dokshitzer, M. Olsson, G. Turnock, B.R. Webber, Phys. Lett. B 269 (1991) 432;
N. Brown, W. Stirling, Z. Phys. C 53 (1992) 629.

[19] G. Borisov, Nucl. Instrum. Methods A 417 (1998) 384;
DELPHI Collaboration, P. Abreu et al., Eur. Phys. J. C 10 (1999) 415.

[20] Yu.L. Dokshitzer, G.D. Leder, S. Moretti, B.R. Webber, JHEP 08 (1997) 001.

[21] L. Lönnblad, Z. Phys. C 58 (1993) 471.

[22] G. Rudolph, ALEPH HERWIG tuning, private communication.

[23] N. Kjaer, M. Mulders, CERN-OPEN-2001-026 (2001).

[24] LEP Energy Working Group, Eur. Phys. J. C 11 (1999) 573;
LEP Energy Working Group, LEP Energy working group note 99/01 (1999).

[25] A. Valassi, Bose–Einstein correlations in W decays, hep-ex/0009039, to be published in the proceedings of the 30th International Conference On High-Energy Physics, Osaka, Japan, 27 July – 2 August 2000.

[26] L. Lönnblad, T. Sjöstrand, Eur. Phys. J. C 2 (1998) 165.

[27] V. Kartvelishvili, R. Kvatadze, R. Møller, Phys. Lett. B 408 (1997) 331.

[28] S. Todorova, J. Rames, IReS-97-29 PRA-HEP-97-16, hep-ph/9710280.

[29] P. de Jong, Color reconnection in W decays, hep-ex/0103018, to be published in the proceedings of the 30th International Conference On High-Energy Physics, Osaka, Japan, 27 July – 2 August 2000.

[30] OPAL Collaboration, G. Abbiendi et al., Eur. Phys. J. C 11 (1999) 217.

[31] T. Sjostrand, V. Khoze, Z. Phys. C 62 (1994) 281;
T. Sjostrand, V. Khoze, Phys. Rev. Lett. 72 (1994) 28.